Non-Hermitian Mott Skin Effect

Tsuneya Yoshida,[1,2] Song-Bo Zhang,[3,4] Titus Neupert,[5] and Norio Kawakami[6,7,8]
[1]Department of Physics, Kyoto University, Kyoto 606-8502, Japan
[2]Institute for Theoretical Physics, ETH Zürich, 8093 Zürich, Switzerland
[3]Hefei National Laboratory, Hefei, Anhui, 230088, China
[4]International Center for Quantum Design of Functional Materials (ICQD), University of Science and Technology of China, Hefei, Anhui 230026, China
[5]Department of Physics, University of Zürich, Winterthurerstrasse 190, 8057 Zürich, Switzerland
[6]Department of Materials Engineering Science, Osaka University, Toyonaka 560-8531, Japan
[7]Department of Physics, Ritsumeikan University, Kusatsu, Shiga 525-8577, Japan
[8]Fundamental Quantum Science Program, TRIP Headquarters, RIKEN, Wako 351-0198, Japan

(Received 28 September 2023; revised 17 April 2024; accepted 24 June 2024; published 14 August 2024)

We propose a novel type of skin effects in non-Hermitian quantum many-body systems that we dub a "non-Hermitian Mott skin effect." This phenomenon is induced by the interplay between strong correlations and the non-Hermitian point-gap topology. The Mott skin effect induces extreme sensitivity to the boundary conditions only in the spin degree of freedom (i.e., the charge distribution is not sensitive to boundary conditions), which is in sharp contrast to the ordinary non-Hermitian skin effect in noninteracting systems. Concretely, we elucidate that a bosonic non-Hermitian chain exhibits the Mott skin effect in the strongly correlated regime by closely examining an effective Hamiltonian. The emergence of the Mott skin effect is also supported by numerical diagonalization of the bosonic chain. The difference between the ordinary non-Hermitian skin effect and the Mott skin effect is also reflected in the time evolution of physical quantities; under the time evolution spin accumulation is observed while the charge distribution remains spatially uniform.

DOI: 10.1103/PhysRevLett.133.076502

Introduction—Since the discovery of topological insulators, extensive efforts have been devoted to understanding topological aspects of condensed matter systems [1–9]. While topological insulators are originally reported for free fermions, it has turned out that the interplay between strong correlations and nontrivial topology triggers further exotic phenomena [10–32]. For instance, strong correlations can induce fractional quantum Hall states [10,11,15,20–25]. Furthermore, topological Mott insulators exhibit the unique bulk-edge correspondence due to the interplay between correlations and the nontrivial topology [33–35]. Namely, corresponding to the nontrivial topology in the bulk, gapless edge modes emerge only in the spin excitation spectrum (i.e., the charge excitation spectrum is gapped even around edges).

Along with the above progress, the topological band theory of non-Hermitian systems has been developed [36–67] and revealed unique phenomena due to the non-Hermitian point-gap topology that do not have Hermitian counterparts [68–82]. A representative example is the non-Hermitian skin effect [83–106] that results in the novel bulk-edge correspondence unique to non-Hermitian systems; because of the nontrivial point-gap topology in the bulk, the eigenstates and eigenvalues exhibit extreme sensitivity to the presence or absence of boundaries [91,92]. Especially, in one-dimensional systems, most of eigenstates are localized only around one of the edges under open boundary conditions (OBC), while they extend into the bulk under periodic boundary conditions (PBC). The above localized eigenstates are known as skin modes.

The above progress on correlated systems and the noninteracting non-Hermitian topology naturally leads us to the following crucial question: *how do strong correlations affect the non-Hermitian skin effects?* The significance of this issue is further enhanced by recent advances in experiments with cold atoms [107–110] and quantum circuits [111] where both dissipation and correlations can be introduced. Correlation effects on the non-Hermitian topological properties have been studied extensively [112–143], but not on non-Hermitian skin effects, which is particularly the case for bosonic systems.

In this Letter, we address this question for a one-dimensional bosonic system and discover a novel type of skin effects, a "non-Hermitian Mott skin effect," which induces striking skin modes. Namely, the nontrivial point-gap topology results in the skin modes in which only the spin degree of freedom is involved (i.e., charges are distributed uniformly even under OBC). This behavior is in sharp contrast to non-Hermitian skin effects in noninteracting systems where bosons are localized around the

edge. We elucidate the emergence of the Mott skin effect by examining an effective spin model in the strong correlation regime, which hosts skin modes and possesses the nontrivial point-gap topology characterized by the spin winding number. We also support the emergence of the Mott skin effect by employing numerical diagonalization. Our numerical analysis also elucidates unique real-time dynamics induced by the Mott skin effect; dynamical spin accumulation is observed while the charge distribution remains spatially uniform.

Model—Let us consider a one-dimensional chain of interacting bosons. The Hamiltonian reads

$$\hat{H} = \hat{H}_0 + \hat{H}_{\mathrm{int}}, \tag{1}$$

$$\hat{H}_0 = \sum_{j\sigma}(-t_{\mathrm{R}\sigma}\hat{b}^\dagger_{j+1\sigma}\hat{b}_{j\sigma} - t_{\mathrm{L}\sigma}\hat{b}^\dagger_{j\sigma}\hat{b}_{j+1\sigma}), \tag{2}$$

$$\hat{H}_{\mathrm{int}} = -\mathrm{i}V\sum_{j\sigma}\hat{n}_{j\sigma}(\hat{n}_{j\sigma}-1) - \mathrm{i}U\sum_{j}\hat{n}_{j\uparrow}\hat{n}_{j\downarrow}, \tag{3}$$

where $\hat{b}^\dagger_{j\sigma}$ ($\hat{b}_{j\sigma}$) creates (annihilates) a boson at site $j = 0, 1, 2\ldots, L-1$ and in the spin state $\sigma = \uparrow, \downarrow$ [144]. The nonreciprocal hopping integrals are denoted by $t_{\mathrm{R}\uparrow} = t_{\mathrm{L}\downarrow} = t_+$ and $t_{\mathrm{L}\uparrow} = t_{\mathrm{R}\downarrow} = t_-$ with real numbers t_+ and t_-. The operator $\hat{n}_{j\sigma}$ denotes the number operator of bosons of spin σ at site j; $\hat{n}_{j\sigma} \coloneqq \hat{b}^\dagger_{j\sigma}\hat{b}_{j\sigma}$. The first (second) term of $\hat{H}_{\mathrm{int}}$ describes the on-site interaction between bosons with the same (opposite) spin. The parameters V and U are nonnegative numbers. Without loss of generality, we assume the relation $t_+ > t_-$ throughout this Letter.

Symmetry and topological invariant—The above model preserves charge U(1) symmetry and spin U(1) symmetry, as indicated by

$$[\hat{H}, \hat{N}] = 0, \tag{4}$$

$$[\hat{H}, \hat{S}^z] = 0, \tag{5}$$

with $\hat{N} = \hat{N}_\uparrow + \hat{N}_\downarrow$ and $2\hat{S}^z = \hat{N}_\uparrow - \hat{N}_\downarrow$. Here, $\hat{N}_\sigma$ denotes the number operator of bosons in the spin state σ; $\hat{N}_\sigma = \sum_j \hat{n}_{j\sigma}$ ($\sigma = \uparrow, \downarrow$). Therefore, the Hamiltonian can be block-diagonalized into $N_\uparrow$ and $N_\downarrow$ sectors. We denote eigenvalues of $\hat{N}_\uparrow$ and $\hat{N}_\downarrow$ as $N_\uparrow$ and $N_\downarrow$, respectively.

In order to characterize the point-gap topology [145], we introduce the many-body spin winding number

$$W_{\mathrm{s}} = \int_0^{2\pi}\frac{d\theta_{\mathrm{s}}}{2\pi\mathrm{i}}\frac{\partial}{\partial\theta_{\mathrm{s}}}\log\left[\det\left(\hat{H}_{[N_\uparrow,N_\downarrow]}(\theta_{\mathrm{s}}) - E_{\mathrm{ref}}\right)\right], \tag{6}$$

which is a variant of the previously introduced many-body winding number [132–134]. Here, in order to compute W_{s}, we have imposed twisted boundary conditions where the twist angle of the down-spin state $\theta_\downarrow$ is opposite to that of the up-spin state $\theta_\uparrow$ [146]; $\hat{b}^\dagger_{0\sigma}\hat{b}_{L-1\sigma} \to e^{\mathrm{i}\theta_\sigma}\hat{b}^\dagger_{0\sigma}\hat{b}_{L-1\sigma}$ with $(\theta_\uparrow, \theta_\downarrow) = (\theta_{\mathrm{s}}, -\theta_{\mathrm{s}})$ and the twist angle θ_{s}. For the Fock space specified by $[N_\uparrow, N_\downarrow]$, the block-diagonalized Hamiltonian is denoted by $\hat{H}_{[N_\uparrow,N_\downarrow]}(\theta_{\mathrm{s}})$. We note that the spin U(1) symmetry is essential for the skin effect; breaking the spin U(1) symmetry destroys the skin effect even for the noninteracting case (see Sec. S2 of Supplemental Material [147]).

Analysis in the strong coupling regime—Before presenting numerical results, we derive an effective model that provides an intuition for the Mott skin effect. In the strong coupling regime (i.e., $V, U \gg t_+, t_-$), the longest lived states of the system are described by an effective spin model, i.e., eigenstates shift in the negative direction of the imaginary axis if bosons occupy the same site, which is attributed to the continuous quantum Zeno effect [148–153].

Applying the second order perturbation theory [154–157] yields the following effective spin model for the states where each site is occupied by one boson:

$$\begin{aligned}\hat{H}_{\mathrm{spin}}(\theta_{\mathrm{s}}) = &\sum_{j=0}^{L-2}\left[J_z\hat{S}^z_{j+1}\hat{S}^z_j + J_+\hat{S}^+_{j+1}\hat{S}^-_j + J_-\hat{S}^-_{j+1}\hat{S}^+_j\right]\\ &+ J_+e^{2\mathrm{i}\theta_{\mathrm{s}}}\hat{S}^+_0\hat{S}^-_{L-1} + J_-e^{-2\mathrm{i}\theta_{\mathrm{s}}}\hat{S}^-_0\hat{S}^+_{L-1} + E_0,\end{aligned} \tag{7}$$

with $J_z = -4\mathrm{i}(t_+t_-)[(1/V) - (1/U)]$, $J_\pm = -2\mathrm{i}(t_\pm^2/U)$, and $E_0 = -\mathrm{i}L(t_+t_-)[(1/V) + (1/U)]$. Here, $\hat{S}^\mu_j$ ($\mu = x, y, z$) denotes spin operators at site j. The spin raising and lowering operators are defined as $S^\pm_j = S^x_j \pm \mathrm{i}S^y_j$. In terms of creation and annihilation operators of bosons, the spin operators are written as $\hat{S}^z_j = (\hat{n}_{j\uparrow} - \hat{n}_{j\downarrow})/2$, $\hat{S}^+_j = \hat{b}^\dagger_{j\uparrow}\hat{b}_{j\downarrow}$, and $\hat{S}^-_j = \hat{b}^\dagger_{j\downarrow}\hat{b}_{j\uparrow}$ for the subspace where each site is occupied by one boson. Details of the derivation are provided in Sec. S1 of Supplemental Material [147]. The above Hamiltonian (7) preserves the spin U(1) symmetry and can be block-diagonalized with S^z, the eigenvalue of $\hat{S}^z = \sum_j \hat{S}^z_j$.

Applying the Jordan-Wigner transformation elucidates that the effective model (7) gives rise to the Mott skin effect (for the detailed derivation, see Sec. S1 of Supplemental Material [147]); the spin model [Eq. (7)] can be mapped to the following spinless fermion model:

$$\begin{aligned}\hat{H}_{\mathrm{spin}}(\theta) = &\sum_{j=0}^{L-2}\left(J_+\hat{f}^\dagger_{j+1}\hat{f}_j + J_-\hat{f}^\dagger_j\hat{f}_{j+1}\right)\\ &- (-1)^{\hat{N}^{\mathrm{f}}}\left(J_+e^{2\mathrm{i}\theta_{\mathrm{s}}}\hat{f}^\dagger_0\hat{f}_{L-1} + J_-e^{-2\mathrm{i}\theta_{\mathrm{s}}}\hat{f}^\dagger_{L-1}\hat{f}_0\right)\\ &+ J_z\sum_{j=0}^{L-1}\hat{n}^{\mathrm{f}}_{j+1}\hat{n}^{\mathrm{f}}_j - J_z\left(\hat{N}^{\mathrm{f}} - \frac{L}{4}\right) + E_0,\end{aligned} \tag{8}$$

with $\hat{N}^{\mathrm{f}} = \sum_j \hat{n}^{\mathrm{f}}_j$, $\hat{S}^+_j = e^{\mathrm{i}\pi\hat{N}^<_j}\hat{f}^\dagger_j$, and $\hat{S}^z_j = (\hat{n}^{\mathrm{f}}_j - \frac{1}{2})$. Here, $\hat{N}^<_j$ and $\hat{n}^{\mathrm{f}}_j$ are defined as $\hat{N}^<_j = \sum_{j=0}^{L-1}\hat{n}^{\mathrm{f}}_j$ and $\hat{n}^{\mathrm{f}}_j = \hat{f}^\dagger_j\hat{f}_j$.

Operators $\hat{f}_j^\dagger$ ($\hat{f}_j$) create (annihilate) a spinless fermion at site j.

In particular, for the subspace with $S^z = 1 - (L/2)$ (i.e., $[N_\uparrow, N_\downarrow] = [1, L-1]$), there exists only one fermion created by $\hat{f}_j^\dagger$. Therefore, the above Hamiltonian is simplified as

$$\hat{H}_{\rm spin}(\theta) = \sum_{j=0}^{L-2} \left(J_+ \hat{f}_{j+1}^\dagger \hat{f}_j + J_- \hat{f}_j^\dagger \hat{f}_{j+1}\right) + \left(J_+ e^{2i\theta_s} \hat{f}_0^\dagger \hat{f}_{L-1} + J_- e^{-2i\theta_s} \hat{f}_{L-1}^\dagger \hat{f}_0\right) + J_z\left(\frac{L}{4} - 1\right) + E_0. \tag{9}$$

This model is nothing but the Hatano-Nelson chain [43,44], which exhibits the skin effect. Specifically, substituting the Hamiltonian (9) to $\hat{H}_{[1,L-1]}(\theta_s)$, we obtain the winding number $W_s = 2$ for the subspace with $[N_\uparrow, N_\downarrow] = [1, L-1]$. Here, we have set the reference energy $E_{\rm ref}$ located inside of the loop formed by the eigenvalues. We recall that $iJ_+ > iJ_-$ holds for $t_+ > t_-$ [see below Eq. (7)]. Corresponding to this nontrivial point-gap topology, skin modes emerge only around the right edge, which are described by fermions created by $\hat{f}_j^\dagger$. J_+ and J_- of the effective Hamiltonian are purely imaginary.

Recalling the relation between spin operators and operators $\hat{f}_j^\dagger$, we can conclude that the system exhibits the Mott skin effect. Namely, only the spin degree of freedom is involved in the skin modes induced by the nontrivial point-gap topology.

Numerical results: Noninteracting case—In order to numerically analyze this model, we employ exact diagonalization. Unless otherwise noted, we set $(t_+, t_-) = (1, 0.1)$.

In the noninteracting case, the system is decomposed into two bosonic Hatano-Nelson models where the hopping in the right (left) direction is dominant for $\sigma = \uparrow$ ($\sigma = \downarrow$). Such nonreciprocal hoppings result in the ordinary non-Hermitian skin effect as discussed below. In the following, we analyze the many-body Hamiltonian (1) for the Fock space with $(N_\uparrow, N_\downarrow) = (1, L-1)$ and $L = 6$ (for an analysis of the one-body Hamiltonian, see Sec. S2 of Supplemental Material [147]).

Figure 1(a) displays the spectral flow of $\hat{H}(\theta_s)$ for $0 \le \theta_s \le 2\pi$, where $E_m(\theta_s)$ $(m = 0, 1, 2, \ldots)$ [158] are eigenvalues of $\hat{H}(\theta_s)$. In this figure, we can see that the spectral flow forms the loop structure, which indicates the point-gap topology characterized by the many-body spin winding number taking a nonzero value for $E_{\rm ref} = -0.01i$ (for more details, see Sec. S3A of Supplemental Material [147]).

Corresponding to this nontrivial point-gap topology, the spectrum shows extreme sensitivity to the boundary

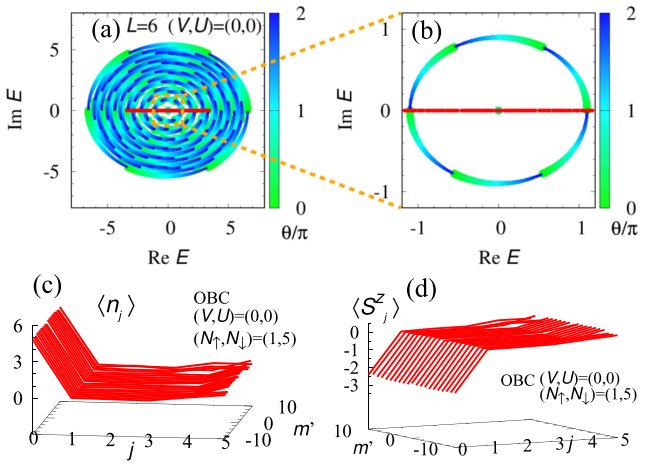

FIG. 1. Energy eigenvalues and expectation values for $V = U = 0$. (a) Energy eigenvalues under twisted boundary conditions and OBC (red), respectively. (b) A magnified version of the range $-1.2 \le \mathrm{Im}E \le 1.2$. The data obtained under OBC are represented by red dots. With increasing θ_s from 0 to 2π, the eigenvalues wind around the origin of the complex plane, which indicates W_s takes a nonzero value for $E_{\rm ref} = -0.01i$. (c) [(d)] Expectation values $\langle \hat{n}_j \rangle$ [$\langle \hat{S}_j^z \rangle$] at each site under OBC. The expectation values are computed from right eigenvectors of the many-body Hamiltonian whose eigenvalues $E_{m'}$ are located around the origin of the complex plane. Specifically, m' is defined as $m' = m - 756$ (for the definition of m, see footnote [158]). We note that the other states show essentially the same behaviors. For $U = V = 0$, the eigenvalues are aligned on the real axis, and the eigenvalues are numerically zero for $m = 756$ ($|E_{756}| < 1 \times 10^{-12}$). These data are obtained for the subspace with $(N_\uparrow, N_\downarrow) = (1, 5)$ and for $(t_+, t_-) = (1, 0.1)$ and $L = 6$.

conditions. Imposing OBC significantly changes the spectrum of $\hat{H}$; as shown in Fig. 1(a), the eigenvalues under OBC are aligned on the real axis in contrast to the eigenvalues under PBC. Eigenstates also show such sensitivity to the boundary conditions [159]. In order to show this, we compute the expectation values of $\hat{n}_j = \sum_\sigma \hat{n}_{j\sigma}$

$$\langle \hat{n}_j \rangle = \frac{{}_{\rm R}\langle \Psi_m | \hat{n}_j | \Psi_m \rangle_{\rm R}}{{}_{\rm R}\langle \Psi_m | \Psi_m \rangle_{\rm R}}, \tag{10}$$

with $|\Psi_m\rangle_{\rm R}$ $(m = 0, 1, 2, \ldots)$ being right eigenvectors of the many-body Hamiltonian [160,161], $\hat{H}|\Psi_m\rangle_{\rm R} = E_m|\Psi_m\rangle_{\rm R}$. As displayed in Fig. 1(c), the bosons are localized around edges under OBC in contrast to the case of PBC (the data for PBC are provided in Sec. S3B of Supplemental Material [147]).

Because of the localization of bosons, a spin polarization is observed only in the presence of boundaries. Figure 1(c) displays the expectation values of $\hat{S}_j^z = (\hat{n}_{j\uparrow} - \hat{n}_{j\downarrow})/2$. The spin polarization is observed under OBC in contrast to the case of PBC.

As discussed above, in the noninteracting cases, the system shows the non-Hermitian skin effect that results in extreme sensitivity of the eigenvalues and eigenstates to the presence or absence of the boundaries. Accordingly, the localization of bosons is observed only under OBC.

Numerical results: Interacting case—Now, we demonstrate that the interplay between strong correlations and nonreciprocal hoppings induces the Mott skin effect. Namely, the nontrivial point-gap topology results in extreme sensitivity to the boundary conditions only in the spin degree of freedom. The spin-charge separation plays an essential role in the emergence of the Mott skin effect. In the following, we focus on the Fock space with $(N_\uparrow, N_\downarrow) = (1, L-1)$ [162]. The Mott skin effect is also observed for other subspaces of half-filling (see Sec. S3C of Supplemental Material [147]).

Figures 2(a) and 2(b) display the spectral flow of $\hat{H}(\theta_s)$ for $(V, U) = (20, 10)$ with increasing θ_s from 0 to 2π. The interactions V and U shift most of the loops in the negative direction of the imaginary axis [see Fig. 2(a)]. However, one of the loops remains around the origin of the complex plane [see Fig. 2(b)]. This is because bosons do not feel the on-site interactions unless multiple bosons occupy the same site.

The states remaining around the origin of the complex plane exhibit the Mott skin effect. Because of the loop

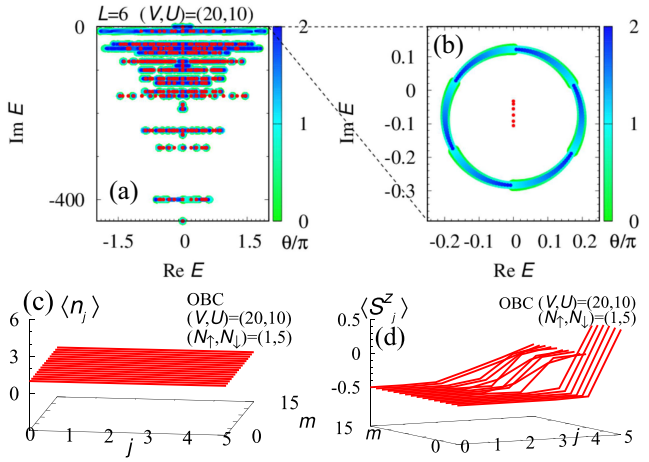

FIG. 2. Energy eigenvalues and expectation values for $(V, U) = (20, 10)$. (a) Energy eigenvalues under twisted boundary conditions and OBC, respectively. (b) A magnified version of the range $-0.39 \leq \mathrm{Im}E \leq 0.19$. In these figures the data obtained under OBC are represented by red dots. With increasing θ_s from 0 to 2π, the eigenvalues wind around the origin of the complex plane, which indicates $W_s = 2$ for $E_{\mathrm{ref}} = -0.01\mathrm{i}$. (c) [(d)] Expectation values $\langle \hat{n}_j \rangle$ [$\langle \hat{S}^z_j \rangle$] at each site under OBC. Here, the expectation values are plotted for eigenstates whose eigenvalues [158] satisfy $-10.02 < \mathrm{Im}E_m < -0.033$. The eigenvalues for $m = 0, \ldots, L-1$ are plotted in panel (b). As is the case of $V = U = 0$, the expectation values are computed from the right eigenvectors (see Fig. 1). These data are obtained for $(t_+, t_-) = (1, 0.1)$ and $L = 6$.

structure, the many-body spin winding number takes $W_s = 2$ for $E_{\mathrm{ref}} = -0.01\mathrm{i}$ (for more details, see Sec. S3A of Supplemental Material [147]). Corresponding to the nontrivial point-gap topology, eigenstates exhibit extreme sensitivity to the presence or absence of boundaries.

Under OBC, eigenvalues plotted in Fig. 2(b) are purely imaginary in contrast to the case of PBC where eigenvalues are distributed on the complex plane. This behavior is understood in terms of $\hat{H}_{\mathrm{spin}}$ [Eq. (9)] which is essentially the Hatano-Nelson chain with pure imaginary hoppings.

Such sensitivity to the boundary conditions is also observed for eigenstates. However, only the spin degree of freedom is involved in the sensitivity of the boundary conditions, which is in sharp contrast to the noninteracting case. Figure 2(c) displays the expectation values $\langle \hat{n}_j \rangle$. As shown in this figure, strong correlations prevent bosons from localizing around the edges, which suppresses the sensitivity to the boundary conditions for the charge degree of freedom. Instead, the spin degree of freedom exhibits extreme sensitivity to the boundary conditions. Figure 2(d) displays the expectation values $\langle \hat{S}^z_j \rangle$. As shown in this figure, the spin polarization is observed under OBC in contrast to the case of PBC (the data for PBC are provided in Sec. S3B of Supplemental Material [147]).

The above results reveal that the system exhibits the Mott skin effect resulting in extreme sensitivity to the boundary conditions only in the spin degree of freedom (i.e., such sensitivity is not observed in the charge degree of freedom). The emergence of the Mott skin effect is due to the interplay between strong correlations and non-Hermitian point-gap topology. We note that the Mott skin effect is observed also for the subspace with $(N_\uparrow, N_\downarrow) = (2, 4)$ and $L = 6$ (for more details see Sec. S3C of Supplemental Material [147]).

Real-time dynamics—As seen above, the Mott skin effect involves only the spin degree of freedom in contrast to the skin effect in the noninteracting case. This difference is also reflected in the time-evolution of physical quantities.

Let us start with the noninteracting case. Figure 3(a) displays the expectation values

$$\langle \hat{n}_j(t) \rangle = \frac{\langle \Phi(t) | \hat{n}_j | \Phi(t) \rangle}{\langle \Phi(t) | \Phi(t) \rangle}, \tag{11}$$

with $|\Phi(t)\rangle = e^{-\mathrm{i}\hat{H}t}|\Phi(0)\rangle$ and t being time [163]. The initial state is chosen so that all of the bosons occupy site $j = 0$; $\sqrt{(L-1)!}|\Phi(0)\rangle = \hat{b}^\dagger_{0\uparrow}(\hat{b}^\dagger_{0\downarrow})^{L-1}|0\rangle$. Figure 3(a) indicates that the bosons remain localized around the left edge due to the skin effect [164]. Figure 3(b) indicates that the above localization is also observed in the expectation values $\langle S^z_j(t) \rangle = \langle \Phi(t) | \hat{S}^z_j | \Phi(t) \rangle / \langle \Phi(t) | \Phi(t) \rangle$. This is because bosons with spin-up (spin-down) are localized around the right (left) edge (see Sec. S2A of Supplemental

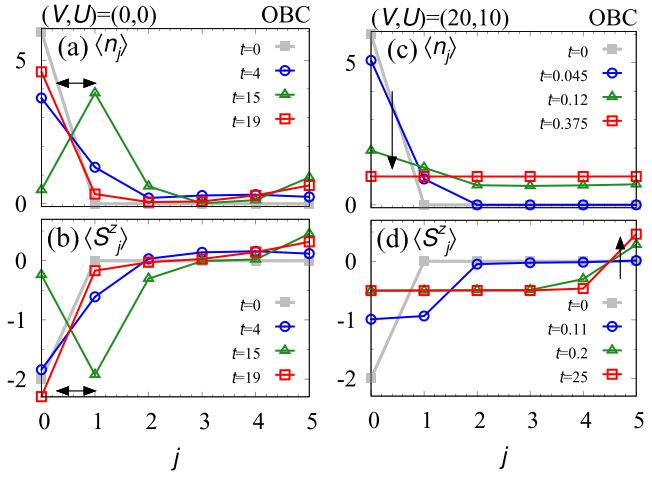

FIG. 3. (a),(c) [(b),(d)] The time evolution of the expectation values $\langle \hat{n}_j(t) \rangle$ [$\langle \hat{S}^z_j(t) \rangle$] under OBC [see Eq. (11)]. Panels (a) and (b) [(c) and (d)] display data for $(V, U) = (0, 0)$ [$(V, U) = (20, 10)$]. These data are obtained for $(t_+, t_-) = (1, 0.1)$ and $L = 6$.

Material [147]). The above results demonstrate that in the noninteracting case, the dynamical properties of the spin degree of freedom are tied to those of charge degree of freedom.

Now, we turn to the real-time dynamics in the correlated case. In contrast to the noninteracting case, dynamics of the spin degree of freedom exhibit an essential difference from those of the charge degree of freedom. Figure 3(c) displays the time evolution of $\langle \hat{n}_j(t) \rangle$ for $(V, U) = (20, 10)$. As seen in Fig. 3(c), bosons immediately extend to the bulk. In particular, for $0.375 \lesssim t$, each site is occupied by one boson. This is because the states where each site is occupied by one boson have a longer lifetime $\tau \sim 1/\mathrm{Im}E_m$ than others. Contrary to the above behavior, the dynamics of the spin degree of freedom exhibit a signal of skin modes. The time evolution of $\langle \hat{S}^z_j \rangle$ is plotted in Fig. 3(d). In this figure, dynamical spin accumulation is observed for $0.2 \lesssim t$. This behavior is observed only under OBC (for data under PBC, see Sec. S3D of Supplemental Material [147]).

As seen above, the Mott skin effect induces the dynamical spin accumulation while the charge degree of freedom remains spatially uniform. These dynamical properties in the strongly correlated case are in sharp contrast to those in the noninteracting case. The above dynamical properties are considered to be observed for open quantum systems even in the presence of quantum jumps.

Conclusion—We have proposed a non-Hermitian Mott skin effect induced by the interplay between strong correlations and the non-Hermitian point-gap topology. In contrast to the ordinary non-Hermitian skin effect, the Mott skin effect results in extreme sensitivity to the boundary conditions only in the spin degree of freedom. We have demonstrated the emergence of the Mott skin effect by analyzing the bosonic non-Hermitian Hamiltonian with nonreciprocal hoppings and on-site interactions. The difference from the ordinary skin effect is also reflected in the dynamical properties; spin accumulation is observed while charge distribution remains spatially uniform.

We finish this Letter with a remark on the relevance to open quantum systems described by the Lindblad equation [165–167]. In this Letter, we have analyzed the non-Hermitian Hamiltonian as a toy model. We note, however, that our Hamiltonian is relevant to an open quantum system having particle losses, and that the above dynamical spin accumulation can be observed even under the presence of the jump term (for more details, see Sec. S4 of Supplemental Material [147]). This fact implies that open quantum systems such as cold atoms with strong correlations may provide a feasible platform to observe the Mott skin effect. Section S4 also provides data of polarizations that serve as a phase diagram for the Mott skin effect. Specifically, Fig. S13 displays polarizations of an Hamiltonian that is essentially the same as the one in Eq. (1).

Note added—While finishing this Letter, we noticed Ref. [168] posted on arXiv, which has some overlap with our results.

Acknowledgments—T. Y. thanks Manfred Sigrist for fruitful discussion. T. Y. particulary thanks Shunsuke Furukawa and Yoshihito Kuno for fruitful discussions on the technical details of exact diagonalization. T. Y. is grateful to the long term workshop YITP-T-23-01 held at YITP, Kyoto University, where a part of this work was done. T. Y. is also grateful for the support from the ETH Pauli Center for Theoretical Studies and the Grant from Yamada Science Foundation. T. N. acknowledges support from the Swiss National Science Foundation through a Consolidator Grant (iTQC, TMCG-2 213805) and a Grant (Project No. 200021E_198011) as part of the FOR 5249 (QUAST) led by the Deutsche Forschungsgemeinschaft (DFG, German Research Foundation). N. K. is supported by the RIKEN TRIP initiative. This work is supported by JSPS Bilateral Program No. JPJSBP120249925, JSPS KAKENHI Grants No. JP21K13850 and No. JP22H05247. S. B. Z. acknowledges the support of the start-up fund at HFNL, the Innovation Program for Quantum Science and Technology (Grant No. 2021ZD0302800), and Anhui Initiative in Quantum Information Technologies (Grant No. AHY170000).

[1] M. Z. Hasan and C. L. Kane, Rev. Mod. Phys. **82**, 3045 (2010).
[2] X.-L. Qi and S.-C. Zhang, Rev. Mod. Phys. **83**, 1057 (2011).

[3] D. J. Thouless, M. Kohmoto, M. P. Nightingale, and M. den Nijs, Phys. Rev. Lett. **49**, 405 (1982).
[4] B. I. Halperin, Phys. Rev. B **25**, 2185 (1982).
[5] Y. Hatsugai, Phys. Rev. Lett. **71**, 3697 (1993).
[6] A. Y. Kitaev, Phys. Usp. **44**, 131 (2001).
[7] C. L. Kane and E. J. Mele, Phys. Rev. Lett. **95**, 146802 (2005).
[8] C. L. Kane and E. J. Mele, Phys. Rev. Lett. **95**, 226801 (2005).
[9] X.-L. Qi, T. L. Hughes, and S.-C. Zhang, Phys. Rev. B **78**, 195424 (2008).
[10] D. C. Tsui, H. L. Stormer, and A. C. Gossard, Phys. Rev. Lett. **48**, 1559 (1982).
[11] R. B. Laughlin, Phys. Rev. Lett. **50**, 1395 (1983).
[12] J. K. Jain, Phys. Rev. Lett. **63**, 199 (1989).
[13] F. D. M. Haldane, Phys. Rev. Lett. **51**, 605 (1983).
[14] F. D. M. Haldane, Phys. Rev. Lett. **55**, 2095 (1985).
[15] X.-G. Wen, Adv. Phys. **44**, 405 (1995).
[16] A. Yu. Kitaev, Ann. Phys. (Amsterdam) **303**, 2 (2003).
[17] X.-G. Wen, *Quantum Field Theory of Many-Body Systems: From the Origin of Sound to an Origin of Light and Electrons* (OUP, Oxford, 2004).
[18] M. A. Levin and X.-G. Wen, Phys. Rev. B **71**, 045110 (2005).
[19] A. Kitaev, Ann. Phys. (Amsterdam) **321**, 2 (2006).
[20] E. Tang, J.-W. Mei, and X.-G. Wen, Phys. Rev. Lett. **106**, 236802 (2011).
[21] K. Sun, Z. Gu, H. Katsura, and S. Das Sarma, Phys. Rev. Lett. **106**, 236803 (2011).
[22] T. Neupert, L. Santos, C. Chamon, and C. Mudry, Phys. Rev. Lett. **106**, 236804 (2011).
[23] D. N. Sheng, Z.-C. Gu, K. Sun, and L. Sheng, Nat. Commun. **2**, 389 (2011).
[24] N. Regnault and B. A. Bernevig, Phys. Rev. X **1**, 021014 (2011).
[25] E. J. Bergholtz and Z. Liu, Int. J. Mod. Phys. B **27**, 1330017 (2013).
[26] L. Fidkowski and A. Kitaev, Phys. Rev. B **81**, 134509 (2010).
[27] A. M. Turner, F. Pollmann, and E. Berg, Phys. Rev. B **83**, 075102 (2011).
[28] L. Fidkowski and A. Kitaev, Phys. Rev. B **83**, 075103 (2011).
[29] Z.-C. Gu and X.-G. Wen, Phys. Rev. B **90**, 115141 (2014).
[30] H. Yao and S. Ryu, Phys. Rev. B **88**, 064507 (2013).
[31] S. Ryu and S.-C. Zhang, Phys. Rev. B **85**, 245132 (2012).
[32] X.-L. Qi, New J. Phys. **15**, 065002 (2013).
[33] D. Pesin and L. Balents, Nat. Phys. **6**, 376 (2010).
[34] S. R. Manmana, A. M. Essin, R. M. Noack, and V. Gurarie, Phys. Rev. B **86**, 205119 (2012).
[35] T. Yoshida, R. Peters, S. Fujimoto, and N. Kawakami, Phys. Rev. Lett. **112**, 196404 (2014).
[36] E. J. Bergholtz, J. C. Budich, and F. K. Kunst, Rev. Mod. Phys. **93**, 015005 (2021).
[37] Y. Ashida, Z. Gong, and M. Ueda, Adv. Phys. **69**, 249 (2020).
[38] Z. Gong, Y. Ashida, K. Kawabata, K. Takasan, S. Higashikawa, and M. Ueda, Phys. Rev. X **8**, 031079 (2018).
[39] K. Kawabata, S. Higashikawa, Z. Gong, Y. Ashida, and M. Ueda, Nat. Commun. **10**, 297 (2019).
[40] K. Kawabata, K. Shiozaki, M. Ueda, and M. Sato, Phys. Rev. X **9**, 041015 (2019).
[41] H. Zhou and J. Y. Lee, Phys. Rev. B **99**, 235112 (2019).
[42] S. Lieu, M. McGinley, and N. R. Cooper, Phys. Rev. Lett. **124**, 040401 (2020).
[43] N. Hatano and D. R. Nelson, Phys. Rev. Lett. **77**, 570 (1996).
[44] N. Hatano and D. R. Nelson, Phys. Rev. B **56**, 8651 (1997).
[45] C. M. Bender and S. Boettcher, Phys. Rev. Lett. **80**, 5243 (1998).
[46] T. Fukui and N. Kawakami, Phys. Rev. B **58**, 16051 (1998).
[47] Y. Ashida, S. Furukawa, and M. Ueda, Phys. Rev. A **94**, 053615 (2016).
[48] Y. C. Hu and T. L. Hughes, Phys. Rev. B **84**, 153101 (2011).
[49] K. Esaki, M. Sato, K. Hasebe, and M. Kohmoto, Phys. Rev. B **84**, 205128 (2011).
[50] M. Sato, K. Hasebe, K. Esaki, and M. Kohmoto, Prog. Theor. Phys. **127**, 937 (2012).
[51] S. Diehl, E. Rico, M. A. Baranov, and P. Zoller, Nat. Phys. **7**, 971 (2011).
[52] C.-E. Bardyn, M. A. Baranov, C. V. Kraus, E. Rico, A. İmamoğlu, P. Zoller, and S. Diehl, New J. Phys. **15**, 085001 (2013).
[53] A. Rivas, O. Viyuela, and M. A. Martin-Delgado, Phys. Rev. B **88**, 155141 (2013).
[54] B. Zhu, R. Lü, and S. Chen, Phys. Rev. A **89**, 062102 (2014).
[55] J. C. Budich, P. Zoller, and S. Diehl, Phys. Rev. A **91**, 042117 (2015).
[56] Z. Gong, S. Higashikawa, and M. Ueda, Phys. Rev. Lett. **118**, 200401 (2017).
[57] S. Lieu, Phys. Rev. B **97**, 045106 (2018).
[58] W. B. Rui, Y. X. Zhao, and A. P. Schnyder, Phys. Rev. B **99**, 241110(R) (2019).
[59] M. M. Denner, A. Skurativska, F. Schindler, M. H. Fischer, R. Thomale, T. Bzdusek, and T. Neupert, Nat. Commun. **12** (2021).
[60] D. Nakamura, T. Bessho, and M. Sato, Phys. Rev. Lett. **132**, 136401 (2024).
[61] K. Yokomizo and S. Murakami, Phys. Rev. Lett. **123**, 066404 (2019).
[62] K. Kawabata, N. Okuma, and M. Sato, Phys. Rev. B **101**, 195147 (2020).
[63] F. Tonielli, J. C. Budich, A. Altland, and S. Diehl, Phys. Rev. Lett. **124**, 240404 (2020).
[64] K. Kawabata, K. Shiozaki, and S. Ryu, Phys. Rev. Lett. **126**, 216405 (2021).
[65] S. Sayyad, J. D. Hannukainen, and A. G. Grushin, Phys. Rev. Res. **4**, L042004 (2022).
[66] P.-Y. Chang, J.-S. You, X. Wen, and S. Ryu, Phys. Rev. Res. **2**, 033069 (2020).
[67] C.-T. Hsieh and P.-Y. Chang, SciPost Phys. Core **6**, 062 (2023).
[68] H. Shen, B. Zhen, and L. Fu, Phys. Rev. Lett. **120**, 146402 (2018).
[69] V. Kozii and L. Fu, Phys. Rev. B **109**, 235139 (2024).
[70] T. Yoshida, R. Peters, and N. Kawakami, Phys. Rev. B **98**, 035141 (2018).

[71] H. Zhou, C. Peng, Y. Yoon, C. W. Hsu, K. A. Nelson, L. Fu, J. D. Joannopoulos, M. Soljačić, and B. Zhen, Science **359**, 1009 (2018).
[72] Z. Yang, A. P. Schnyder, J. Hu, and C.-K. Chiu, Phys. Rev. Lett. **126**, 086401 (2021).
[73] J. C. Budich, J. Carlström, F. K. Kunst, and E. J. Bergholtz, Phys. Rev. B **99**, 041406(R) (2019).
[74] R. Okugawa and T. Yokoyama, Phys. Rev. B **99**, 041202 (R) (2019).
[75] H. Zhou, J. Y. Lee, S. Liu, and B. Zhen, Optica **6**, 190 (2019).
[76] T. Yoshida, R. Peters, N. Kawakami, and Y. Hatsugai, Phys. Rev. B **99**, 121101(R) (2019).
[77] T. Yoshida, R. Peters, N. Kawakami, and Y. Hatsugai, Prog. Theor. Exp. Phys. **2020**, 12A109 (2020).
[78] K. Kawabata, T. Bessho, and M. Sato, Phys. Rev. Lett. **123**, 066405 (2019).
[79] J. Carlström, M. Stålhammar, J. C. Budich, and E. J. Bergholtz, Phys. Rev. B **99**, 161115(R) (2019).
[80] Y. Xu, S.-T. Wang, and L.-M. Duan, Phys. Rev. Lett. **118**, 045701 (2017).
[81] P. Delplace, T. Yoshida, and Y. Hatsugai, Phys. Rev. Lett. **127**, 186602 (2021).
[82] I. Mandal and E. J. Bergholtz, Phys. Rev. Lett. **127**, 186601 (2021).
[83] T. E. Lee, Phys. Rev. Lett. **116**, 133903 (2016).
[84] V. M. Martinez Alvarez, J. E. Barrios Vargas, and L. E. F. Foa Torres, Phys. Rev. B **97**, 121401(R) (2018).
[85] S. Yao and Z. Wang, Phys. Rev. Lett. **121**, 086803 (2018).
[86] S. Yao, F. Song, and Z. Wang, Phys. Rev. Lett. **121**, 136802 (2018).
[87] F. K. Kunst, E. Edvardsson, J. C. Budich, and E. J. Bergholtz, Phys. Rev. Lett. **121**, 026808 (2018).
[88] E. Edvardsson, F. K. Kunst, and E. J. Bergholtz, Phys. Rev. B **99**, 081302(R) (2019).
[89] D. S. Borgnia, A. J. Kruchkov, and R.-J. Slager, Phys. Rev. Lett. **124**, 056802 (2020).
[90] C. H. Lee and R. Thomale, Phys. Rev. B **99**, 201103(R) (2019).
[91] K. Zhang, Z. Yang, and C. Fang, Phys. Rev. Lett. **125**, 126402 (2020).
[92] N. Okuma, K. Kawabata, K. Shiozaki, and M. Sato, Phys. Rev. Lett. **124**, 086801 (2020).
[93] N. Okuma and M. Sato, Annu. Rev. Condens. Matter Phys. **14**, 83 (2023).
[94] R. Lin, T. Tai, L. Li, and C. H. Lee, Front. Phys. **18**, 53605 (2023).
[95] L. Xiao, T. Deng, K. Wang, G. Zhu, Z. Wang, W. Yi, and P. Xue, Nat. Phys. **16**, 761 (2020).
[96] T. Helbig, T. Hofmann, S. Imhof, M. Abdelghany, T. Kiessling, L. W. Molenkamp, C. H. Lee, A. Szameit, M. Greiter, and R. Thomale, Nat. Phys. **16**, 747 (2020).
[97] Q. Liang, D. Xie, Z. Dong, H. Li, H. Li, B. Gadway, W. Yi, and B. Yan, Phys. Rev. Lett. **129**, 070401 (2022).
[98] T. Yoshida, T. Mizoguchi, and Y. Hatsugai, Phys. Rev. Res. **2**, 022062 (2020).
[99] R. Okugawa, R. Takahashi, and K. Yokomizo, Phys. Rev. B **102**, 241202(R) (2020).
[100] K. Kawabata, M. Sato, and K. Shiozaki, Phys. Rev. B **102**, 205118 (2020).
[101] Y. Fu and S. Wan, Phys. Rev. B **103**, 045420 (2021).
[102] N. Okuma and M. Sato, Phys. Rev. Lett. **123**, 097701 (2019).
[103] F. Song, S. Yao, and Z. Wang, Phys. Rev. Lett. **123**, 170401 (2019).
[104] T. Haga, M. Nakagawa, R. Hamazaki, and M. Ueda, Phys. Rev. Lett. **127**, 070402 (2021).
[105] F. Yang, Q.-D. Jiang, and E. J. Bergholtz, Phys. Rev. Res. **4**, 023160 (2022).
[106] G. Hwang and H. Obuse, Phys. Rev. B **108**, L121302 (2023).
[107] T. Tomita, S. Nakajima, I. Danshita, Y. Takasu, and Y. Takahashi, Sci. Adv. **3**, e1701513 (2017).
[108] T. Tomita, S. Nakajima, Y. Takasu, and Y. Takahashi, Phys. Rev. A **99**, 031601(R) (2019).
[109] Y. Takasu, T. Yagami, Y. Ashida, R. Hamazaki, Y. Kuno, and Y. Takahashi, Prog. Theor. Exp. Phys. **2020**, 12A110 (2020).
[110] K. Honda, S. Taie, Y. Takasu, N. Nishizawa, M. Nakagawa, and Y. Takahashi, Phys. Rev. Lett. **130**, 063001 (2023).
[111] R. Ma, B. Saxberg, C. Owens, N. Leung, Y. Lu, J. Simon, and D. I. Schuster, Nature (London) **566**, 51 (2019).
[112] T. Yoshida, K. Kudo, and Y. Hatsugai, Sci. Rep. **9**, 16895 (2019).
[113] T. Yoshida, K. Kudo, H. Katsura, and Y. Hatsugai, Phys. Rev. Res. **2**, 033428 (2020).
[114] C.-X. Guo, X.-R. Wang, C. Wang, and S.-P. Kou, Phys. Rev. B **101**, 144439 (2020).
[115] N. Matsumoto, K. Kawabata, Y. Ashida, S. Furukawa, and M. Ueda, Phys. Rev. Lett. **125**, 260601 (2020).
[116] Q. Zhang, W.-T. Xu, Z.-Q. Wang, and G.-M. Zhang, Commun. Phys. **3**, 209 (2020).
[117] C.-X. Guo, X.-R. Wang, and S.-P. Kou, Europhys. Lett. **131**, 27002 (2020).
[118] H. Shackleton and M. S. Scheurer, Phys. Rev. Res. **2**, 033022 (2020).
[119] K. Yang, S. C. Morampudi, and E. J. Bergholtz, Phys. Rev. Lett. **126**, 077201 (2021).
[120] Z. Wang, X.-D. Dai, H.-R. Wang, and Z. Wang, arXiv:2306.12482.
[121] D.-W. Zhang, Y.-L. Chen, G.-Q. Zhang, L.-J. Lang, Z. Li, and S.-L. Zhu, Phys. Rev. B **101**, 235150 (2020).
[122] T. Liu, J. J. He, T. Yoshida, Z.-L. Xiang, and F. Nori, Phys. Rev. B **102**, 235151 (2020).
[123] Z. Xu and S. Chen, Phys. Rev. B **102**, 035153 (2020).
[124] L. Pan, X. Wang, X. Cui, and S. Chen, Phys. Rev. A **102**, 023306 (2020).
[125] W. Xi, Z.-H. Zhang, Z.-C. Gu, and W.-Q. Chen, Sci. Bull. **66**, 1731 (2021).
[126] T. Yoshida and Y. Hatsugai, Phys. Rev. B **104**, 075106 (2021).
[127] T. Yoshida and Y. Hatsugai, Phys. Rev. B **107**, 075118 (2023).
[128] T. Orito and K.-I. Imura, Phys. Rev. B **105**, 024303 (2022).
[129] R. Shen and C. H. Lee, Commun. Phys. **5**, 238 (2022).
[130] S. Mu, C. H. Lee, L. Li, and J. Gong, Phys. Rev. B **102**, 081115(R) (2020).
[131] C. H. Lee, Phys. Rev. B **104**, 195102 (2021).

[132] S.-B. Zhang, M. M. Denner, T. c. v. Bzdušek, M. A. Sentef, and T. Neupert, Phys. Rev. B **106**, L121102 (2022).

[133] K. Kawabata, K. Shiozaki, and S. Ryu, Phys. Rev. B **105**, 165137 (2022).

[134] T. Yoshida and Y. Hatsugai, Phys. Rev. B **106**, 205147 (2022).

[135] F. Alsallom, L. Herviou, O. V. Yazyev, and M. Brzezińska, Phys. Rev. Res. **4**, 033122 (2022).

[136] W. N. Faugno and T. Ozawa, Phys. Rev. Lett. **129**, 180401 (2022).

[137] S. Hamanaka, K. Yamamoto, and T. Yoshida, Phys. Rev. B **108**, 155114 (2023).

[138] S. Tsubota, H. Yang, Y. Akagi, and H. Katsura, Phys. Rev. B **105**, L201113 (2022).

[139] S. Sayyad and J. L. Lado, Phys. Rev. Res. **5**, L022046 (2023).

[140] G. Chen, F. Song, and J. L. Lado, Phys. Rev. Lett. **130**, 100401 (2023).

[141] S. Sayyad, Phys. Rev. Res. **6**, L012028 (2024).

[142] S. Sayyad and J. L. Lado, J. Phys. Condens. Matter **36**, 185603 (2024).

[143] Y. Qin and L. Li, Phys. Rev. Lett. **132**, 096501 (2024).

[144] To be precise, "spin" denotes pseudospin because the system is bosonic. However, for simplicity, we denote it by "spin".

[145] The point-gap of the many-body Hamiltonian opens for $\det(\hat{H}_{[N_\uparrow,N_\downarrow]}(\theta_s) - E_{\mathrm{ref}})$.

[146] This is because the Hamiltonian (1) is decomposed into two bosonic Hatano-Nelson model where the hopping to the right (left) is larger than the other for $\sigma = \uparrow$ ($\sigma = \downarrow$).

[147] See Supplemental Material at http://link.aps.org/supplemental/10.1103/PhysRevLett.133.076502 for details of the perturbation theory and detailed results of the bosonic Hubbard model.

[148] B. Misra and E. C. G. Sudarshan, J. Math. Phys. (N.Y.) **18**, 756 (1977).

[149] W. M. Itano, D. J. Heinzen, J. J. Bollinger, and D. J. Wineland, Phys. Rev. A **41**, 2295 (1990).

[150] M. C. Fischer, B. Gutiérrez-Medina, and M. G. Raizen, Phys. Rev. Lett. **87**, 040402 (2001).

[151] Y.-J. Han, Y.-H. Chan, W. Yi, A. J. Daley, S. Diehl, P. Zoller, and L.-M. Duan, Phys. Rev. Lett. **103**, 070404 (2009).

[152] J. J. García-Ripoll, S. Dürr, N. Syassen, D. M. Bauer, M. Lettner, G. Rempe, and J. I. Cirac, New J. Phys. **11**, 013053 (2009).

[153] M. Nakagawa, N. Kawakami, and M. Ueda, Phys. Rev. Lett. **126**, 110404 (2021).

[154] E. Altman, W. Hofstetter, E. Demler, and M. D. Lukin, New J. Phys. **5**, 113 (2003).

[155] A. B. Kuklov and B. V. Svistunov, Phys. Rev. Lett. **90**, 100401 (2003).

[156] A. Kuklov, N. Prokof'ev, and B. Svistunov, Phys. Rev. Lett. **92**, 050402 (2004).

[157] Ş Söyler, B. Capogrosso-Sansone, N. V. Prokof'ev, and B. V. Svistunov, New J. Phys. **11**, 073036 (2009).

[158] The eigenvalues are labeled by m ($m = 0, 1, 2, \ldots$) so that the following conditions are satisfied: $\mathrm{Im}E_{m+1} < \mathrm{Im}E_m$; if $\mathrm{Im}E_m = \mathrm{Im}E_{m+1}$, m satisfy $\mathrm{Re}E_m \leq \mathrm{Re}E_{m+1}$.

[159] L. Garbe, Y. Minoguchi, J. Huber, and P. Rabl, SciPost Phys. **16**, 029 (2024).

[160] S. S. Roy, S. Bandyopadhyay, R. C. de Almeida, and P. Hauke, arXiv:2309.00049.

[161] There is another way of computing expectation values: using left and right eigenvectors [160]. Because the time evolution is computed from the eigenvalues and the right eigenvectors [see Eq. (11)], we compute the expectation values from the right eigenvectors.

[162] The Mott skin effect is also observed for other subspaces of half-filling $N_\uparrow + N_\downarrow = L$.

[163] We note that postselected real-time dynamics of open quantum systems are described by $i\partial_t|\Phi(t)\rangle = \hat{H}|\Phi(t)\rangle$ [47].

[164] We note that Bloch oscillation is observed around the left edge ($j = 0$) as illustrated by the arrow in Fig. 3(a). This oscillation is due to the interference between skin modes whose time evolution is given by $e^{-i\hat{H}t}|\Phi_m\rangle_R = e^{-iE_m t}|\Phi_m\rangle_R$.

[165] G. Lindblad, Commun. Math. Phys. **48**, 119 (1976).

[166] V. Gorini, A. Kossakowski, and E. C. G. Sudarshan, J. Math. Phys. (N.Y.) **17**, 821 (2008).

[167] H.-P. Breuer and F. Petruccione, *The Theory of Open Quantum Systems* (Oxford University Press, USA, 2002).

[168] B. H. Kim, J.-H. Han, and M. J. Park, arXiv:2309.07894.